Thermoelectric power of some compositions of GeTe-rich $(GeTe)_{1-x}(AgBiTe_2)_x$ solid solutions

1993 J. Phys.: Condens. Matter 5 67

(http://iopscience.iop.org/0953-8984/5/1/008)

J. Phys.: Condens. Matter 5 (1993) 67–84. Printed in the UK

Thermoelectric power of some compositions of GeTe-rich $(GeTe)_{1-x}(AgBiTe_2)_x$ solid solutions

S K Plachkova and T I Georgiev

Faculty of Physics, University of Sofia, Boulevard James Bouchier 5, BG-1126 Sofia, Republic of Bulgaria

Received 31 July 1992

Abstract. A method for preparing single-phase ingots of GeTe-rich solid solutions ($x \leqslant 0.20$) in the system $(GeTe)_{1-x}(AgBiTe_2)_x$ is developed. The temperature dependence (77 to $\simeq$ 900 K) of the thermoelectric power is measured. The curves for GeTe and GeTe-rich solid solutions are of similar shape. Using conventional transport theory, the lattice and electronic contributions to this effect are obtained. To explain the behaviour of diffusion and phonon-drag terms, the metallic expressions for both are used. On the basis of band-edge models of GeTe and $AgBiTe_2$, the non-parabolic two-band Kane model of IV–VI compounds, and separate values of the electronic parts of the thermoelectric power, information about the Fermi energy and degree of degeneracy is obtained. A qualitative interpretation of the temperature dependence of S_e is made.

1. Introduction

It is well known that GeTe and GeTe-rich solid solutions (SS) are strongly degenerate narrow-band-gap semiconductors of p-type conductivity due to the presence of vacancies in the cation sublattice [1]. According to the T–x projection of the Ge–Te phase diagram, the region of the compound

$$(Ge_{1-\delta}V_\delta^c)Te \tag{1}$$

(V_δ^c are the initial 'empty cation sites', i.e. vacancies, and δ is their number) is displaced to the Te-rich side. The high-temperature crystal lattice of GeTe is cubic (NaCl type), with a space group of symmetry O_h^5, but at low temperatures it is rhombohedral, C_{3v}^5 (at Te content less than 50.4 at.%), or orthorhombic, D_{2h}^{16} (at Te content more than 50.4 at.% and $p_c > 1.1 \times 10^{27}$ m^{-3}) [2].

According to the physicochemical investigation of the system $(GeTe)_{1-x}(AgBiTe_2)_x$, a continuous series of SS exists above 773 K, but at lower temperatures the solubility is limited owing to decomposition of $AgBiTe_2$ and SS based on it. The GeTe-rich SS undergoes a reversible O_h^5–C_{3v}^5 phase transition. The phase transition temperature decreases with increasing x from about 700 K for Ge-rich GeTe to room temperature for SS with x about 0.23 [3, 4]. The transport coefficients for this system are investigated for $0 \leqslant x \leqslant 1$ at 300 K (bulk samples) [5] and in the temperature interval from 77 to 700 K (hot-pressed samples of $(GeTe)_{1-2x}(AgBiTe_2)_{2x}$ with $x = 0.05, 0.10, 0.15$) [6]. The temperature dependence of the thermoelectric power S of $(GeTe)_{1-x}(AgBiTe_2)_x$ SS for bulk samples of the alloys with $x = 0.05, 0.10, 0.15$ and 0.20 was measured and discussed earlier [7].

0953-8984/93/010067+18$07.50

The aim of the present paper is to analyse the temperature dependence of the thermoelectric power, measured from 77 to $\simeq$ 900 K, and to obtain information about the Fermi energy (F) and degree of degeneracy of different compositions of GeTe-rich $(GeTe)_{1-x}(AgBiTe_2)_x$ ss.

2. Experimental procedure

The alloys were synthesized from elements with purity 99.999% (Ag, Bi, Te) and 50 Ω cm Ge by melting in ampoules sealed under high (1.3×10^{-4} Pa) vacuum. The ampoules were cleaned, dried and outgased beforehand. The temperature of the furnace was above 1273 K and the reaction continued for about 48 h, the ampoules being continuously vibrated to ensure a thorough mixing of the melt. At the end of the synthesis the ampoules were slowly cooled to a temperature about 100 K below the solidus line of the phase diagram and then they were rapidly cooled in ice–water and annealed at 773 K for 1000 h to reach the equilibrium state.

The thermoelectric power was measured using the method of Steenbeck and Baranskii [8] with an accuracy of about 5%. The temperature difference in the sample was about 5 K. The absolute values of the thermoelectric power were found using the data given in [9].

The temperature dependences of the ss transport coefficients are the result of crystal lattice changes with temperature, the corresponding band-edge changes, and the kind and the degree of degeneracy of the carriers. Because of this, some theoretical considerations must be given first for a better explanation of the observed curves.

3. Theoretical background

3.1. Crystal structure

It is well known that among the IV–VI compounds the tellurides (GeTe and SnTe) and the alloy systems based on them ($Pb_{1-x}Sn_xTe$, $Pb_{1-x}Ge_xTe$, $Sn_{1-x}Ge_xTe$) represent a unique class of displacive ferroelectric semiconductors with a narrow energy gap and a structural phase transition from high-temperature cubic O_h^5 (NaCl type) to rhombohedral C_{3v}^5 (As like) structure at a critical temperature (T_c) [10, 11].

The $(GeTe)_{1-x}(AgBiTe_2)_x$ ss must be considered as pseudo IV–VI compounds. This was established by investigation of the crystal structure and defects of GeTe–Ag_2Te–Bi_2Te_3 ss [12–14]. The exact formula of the $(GeTe)_{1-x}(AgBiTe_2)_x$ ss for its real composition may be written as [10]

$$[(Ge_{(1-x)/(1+x)}Ag_{x/(1+x)}Bi_{x/(1+x)})_{1-\delta}V_\delta^c]Te \qquad (2)$$

and refers to the non-stoichiometric nature of the basic compound GeTe. The number of ionized cation vacancies V^c is δ (see (1)).

As for the IV–VI compounds the rhombohedral distortion of the $(GeTe)_{1-x}(AgBiTe_2)_x$ ss below T_c can be described in terms of three components (see figure 1), as follows:

(i) The optical distortion is a spontaneous static relative shift u in parts of the lattice constant (a) of the two cubic sublattices along the ⟨111⟩ direction, which becomes the rhombohedral c axis. If we denote the atomic coordinates as $(q, q, q) + (000, \frac{1}{2}\frac{1}{2}0, \frac{1}{2}0\frac{1}{2}, 0\frac{1}{2}\frac{1}{2})$ for the cations and $(\bar{q}, \bar{q}, \bar{q}) + (000, \frac{1}{2}\frac{1}{2}0, \frac{1}{2}0\frac{1}{2}, 0\frac{1}{2}\frac{1}{2})$ for the anions, then in the rhombohedral distortion the single-atom position parameter q changes from a value of 0.25 in the cubic phase to $q = 0.25 - \delta$. This means that the sublattice shifts by $x = 2\delta$ along the [100] axis of the FCC lattice or by $u = 2\sqrt{3}\delta$ along the body diagonal (the c axis). It is caused by the softening of the zone-centre transverse optical (TO) phonon mode. As a result of this the inversion symmetry is lost, double cation–anion layers are formed and spontaneous polarization occurs, although this cannot be observed because it is screened by free carriers.

(ii) The acoustic distortion is the homogeneous rhombohedral shear strain ϵ_s, which manifests itself as a change in the inter-axial angle ($2\epsilon_s = \Delta\phi = (\pi/2) - \phi$ in radians) of the unit cell (in the rhombohedral shear strain the cubic lattice is stretched along the rhombohedral c axis and contracted in the perpendicular direction).

(iii) The dilatational strain ϵ_d is due to a change in the lattice constant Δa, or a change δV in the specific volume [10, 11, 15]. The values of the above parameter for C_{3v}^5 GeTe at room temperature are $u = 0.034$, $\epsilon_s \simeq 0.15$ and $\delta V \simeq 0.015$ [1].

3.2. The band structure of IV–VI compounds in cubic and rhombohedral phases

In the narrow-gap semiconductors the interaction between different levels involved in the band structure is small except for those from the conduction and valence bands. Using the kp method leads to a simple two-band Kane model [15] in which the assumption of an ellipsoidal band structure gives an energy–momentum relationship

$$E(E + E_g) = Q_\perp^2 k_\perp^2 + Q_z^2 k_z^2 \tag{3}$$

where $Q_\perp$ and Q_z are the direct transverse and longitudinal valence–conduction band interactions and the coordinate system has been taken with the z axis parallel to the ⟨111⟩ direction of the cubic crystal.

In fact, in the vicinity of the Fermi level, for example of the alloy system $Pb_{1-x}Sn_xTe$, there are six levels clustered in a spread of 4 eV, while the nearest other levels with non-zero kp matrix elements lie about 8 eV from the Fermi level [16]. The consequence is that a six-band model is necessary for an improved kp calculation [17, 18]. Dimmock [18] showed that in the cubic phase the energy–momentum relationship for these IV–VI compounds can be expressed as

$$(E - Ak_\perp^2 - Bk_z^2)(E + E_g - Ck_\perp^2 - Dk_z^2) = Q_\perp^2 k_\perp^2 + Q_z^2 k_z^2 \tag{4}$$

where A, B, C are the contributions from the lower indirect conduction and valence bands, while $Q_\perp, Q_z$ and the coordinate system are the same as those in the Kane model of equation (3). The energy gap, defined as $E_g = E(L_{62}^-) - E(L_{61}^+)$ in the symbols of Mitchell and Wallis [17], was taken by Dimmock [18] to vary linearly with x across the alloy system. Band inversion is included by allowing the energy gaps to take negative values. The result of these calculations is that there are four equivalent valleys at the point L of the cubic Brillouin zone (BZ), which show strong non-parabolicity. Bangert [19] considered the modifications to the Dimmock model that were necessary to take into account the rhombohedral distortion at the structural phase transition. The four equivalent valleys at the L points of the cubic BZ split into a single T valley and three equivalent L valleys. The symmetry of the conduction

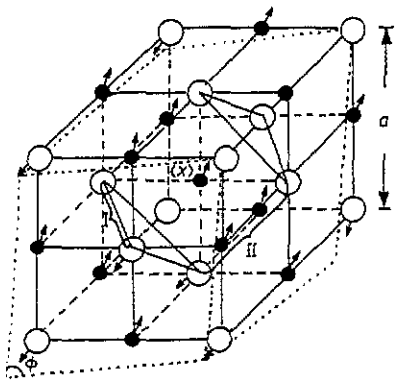

Figure 1. High-temperature rock-salt structure (full and broken lines) and its rhombohedral distortion (dotted lines) at the reversible cubic–rhombohedral phase transition of GeTe and GeTe-rich $(GeTe)_{1-x}(AgBiTe_2)_x$ SS. Full circles—Ge, Ag or Bi cations; open circles—Te anions. Arrows indicate the directions of the movements of the atoms at the phase transition. I and II, respectively, show the distances between the Te atoms (d_{Te-Te}) in the layer (intra-layer Te–Te distances) and between the layers (inter-layer Te–Te distances) in the layered rhombohedral structure. The rhombohedral distortion is characterized by the changes in the inter-axial angle ϕ, and the lattice constant a and the order parameter $\langle x \rangle$.

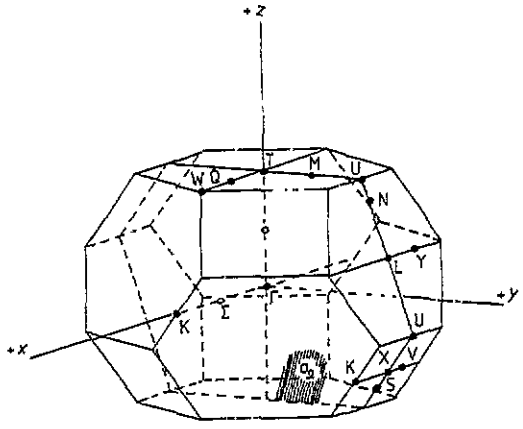

Figure 2. Brillouin zone of the rhombohedral IV–VI compounds showing the notation for the points, lines and planes of symmetry. The mirror plane (σ_0) is perpendicular to the direction of the x axis.

and the valence band states is reduced from D_{3d} to C_{3v} for the T points of the rhombohedral BZ and to C_s for the L points (see figure 2). The structure of the bands in the rhombohedral phase was obtained by changing the lattice periodic potential:

$$V(r) = V_0(r) + V'(r) \tag{5}$$

where $V_0(r)$ is the lattice potential of the cubic phase. $V'(r)$, of C_{3v} symmetry, accounted for the distortion related to the sublattice shift u. For the calculation of the $E(k)$ relationship at the T points, $V'(r)$ was added to the cubic one-electron Hamiltonian H_0. The resulting energy–momentum relationship for the T-point valley was found to be

$$(E - Ak_\perp^2 - Bk_z^2 + nSk_\perp)(E + E_g - Ck_\perp^2 - Dk_z^2 - nSk_\perp) = Q_\perp'^2 k_\perp^2 + Q_z^2 k_z^2 \tag{6}$$

where $n = \pm 1$ for the two 'spin' states (Kramers conjugate pair), A, B, C, D and Q_z are the same parameters as applied in the cubic phase while $Q'_\perp$ are different from the corresponding $Q_\perp$ of equation (4) for the cubic phase, i.e. $Q'_\perp = Q_\perp \cos(2\theta)$. For the parameters E_g and S, Bangert [19] showed that

$$E_g^2 = E_{gc}^2 + 4\Delta^2 \tag{7}$$

$$S \simeq Q \sin(2\theta) \qquad \tan(2\theta) \simeq 2\Delta / E_{gc} \tag{8}$$

where E_g is the energy gap in C_{3v} phase at the T point of the BZ, E_{gc} is the energy gap in the cubic phase and Δ is the matrix element of the lattice potential $V'(r)$ between the conduction and valence band states. For $T > T_c$, $\Delta = 0$. Below T_c, Δ is a function of temperature because of the temperature dependence of $V'(r)$, which results from the order parameter u. The term involving S characterized the C_{3v} distortion symmetry and was linear in $k_\perp$ because it originated from a breaking of the inversion symmetry of the cubic phase. Since Δ is zero in the cubic phase, the Bangert model of equation (6) can be seen to be in agreement with the Dimmock model of equation (4) in this regime.

In order to estimate the shape of the Fermi surfaces, Bauer *et al* [11] neglected the far-band terms in the matrix Hamiltonian. The surfaces of constant energy in this two-band approximation consist of intersecting ellipsoids of revolution. The centres of the ellipsoids are displaced with respect to each other by $2k_0$ ($k_0 = S(E + E_g)/2Q_z^2$). The $E(k)$ relation for the T valley is shown in figure 3 for the case of $Pb_{1-x}Ge_xTe$ [11]. The surfaces of constant energy of $Pb_{0.68}Sn_{0.32}Te$ for $p = 1.1 \times 10^{18}$ cm^{-3} in the rhombohedral phase [20] are presented in figure 4 for the T and L valleys. At the T point the term $\pm Sk_\perp$ has the effect of modifying the single ellipsoid of the Dimmock model as in figure 4, yielding two surfaces—an outer 'skin' (T^+) and an inner 'core' (T^-) of an apple-like object. Furthermore, in the case of the L points, a similar pair of surfaces tilted from the normal to the BZ at L (L^+ and L^-) is expected to be seen).

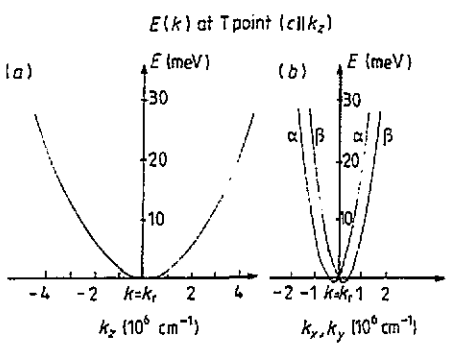

Figure 3. $E(k)$ relation for the T conduction band valley for (*a*) $k \parallel c$ and (*b*) $k \perp c$ for $Pb_{1-x}Ge_xTe$ ($E = F = 30$ meV). The kp parameters used have been determined from the magneto-optical data [11].

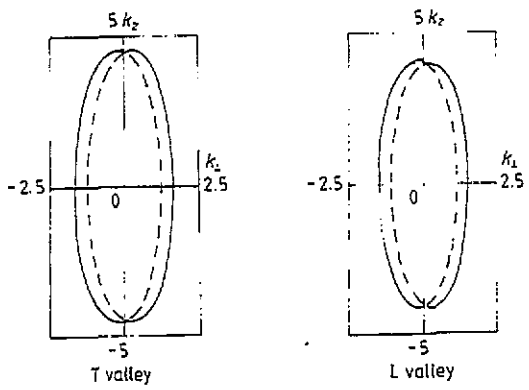

Figure 4. The Fermi surface of $Pb_{0.68}Sn_{0.32}Te$ for $p = 1.1 \times 10^{18}$ cm^{-3} in the rhombohedral phase. The full curves (the + or outer surfaces) and the broken curves (the − or inner surfaces) represent carriers in different 'spin' states. For the T valley k_z is parallel to the rhombohedral c axis, but for the L valley k_z is not normal to the face of the Brillouin zone. $k_\perp^2 = k_x^2 + k_y^2$, i.e. all surfaces have axial symmetry about k_z. The unit of k_z and $k_\perp$ is 10^6 cm^{-1} [20].

In order to obtain the $E(k)$ relationship for finite temperatures, Bangert [21] has taken into account two matrix elements R_1 and R_2 neglected in his zero-temperature calculations [19], which represent contributions from the interband electron–phonon

interactions. The energy–momentum relationship in this case is given by

$$(E-Ak_\perp^2-Bk_z^2+nSk_\perp)(E+E_g-Ck_\perp^2-Dk_z^2-nSk_\perp)=\cos^2(2\theta)Q_\perp^2k_\perp^2+Q_z^2k_z^2 \tag{9}$$

where

$$S=Q_\perp\sin(2\theta) \qquad n=\pm 1 \tag{10}$$

and

$$\tan(2\theta)=2\Delta/[E_{gc}-(R_1+R_2)]. \tag{11}$$

Δ is related to the optical deformation potential Ξ by

$$\Delta=\Xi u \tag{12}$$

with u being the relative sublattice displacement. The energy gap E_g in the rhombohedral phase at the T point is related to the energy gap in the cubic phase E_{gc} by

$$E_g^2=(E_{gc}+R_1-R_2)^2+4\Delta^2. \tag{13}$$

Comparing the dispersion relationship of the zero-temperature (equation (6)) and the finite-temperature (equation (9)) Bangert models, three differences are apparent:

(i) Taking R_1 and R_2 into account, the $k_\perp^2$ terms ($Q'_\perp$) will be temperature-dependent at $T<T_c$, which means that the electron–phonon coupling changes not only the band gap but also the direct band interactions ($Q'_\perp$).

(ii) The band gap E_g will take into account not only Δ, the contribution from the interband electron–optical phonon interactions (see equation (7)), but also R_1 and R_2, the contributions from the interband acoustic coupling (see equation (13)).

(iii) S will be exactly, not approximately, equal to $Q_\perp\sin(2\theta)$ (see equations (8) and (10)).

The model can be extended to involve the case of the band inversion transition (the position of the bands in SnTe and GeTe are inverted with respect to the bands in PbTe) [20] if $E_g=E(L_6^-)-E(L_6^+)$ and equation (13) is rewritten as

$$E_g=(|E_{gc}|/E_{gc})[(|E_{gc}|+R_1-R_2)^2+4\Xi^2u^2]^{1/2}. \tag{14}$$

This model is called the modified Bangert model.

It is well known that in a cubic crystal the band edge at the nth valley shifts with strain by an amount [22]

$$\delta E_n=\sum D_{ij}^n\epsilon_{ij} \qquad D_{ij}^n=D_d\delta_{ij}+D_u a_i a_j \tag{15}$$

where ϵ_{ij} is the strain tensor component, D_u and D_d are respectively the shear and dilatation deformation potentials and the a_i or a_j are direction cosines of the angles between the major axis of the nth valley and the cubic axis. Using equation (15), the band-edge shifts due to the rhombohedral shear strain ($\epsilon_{ij}=\epsilon_{ji}=\epsilon_s>0$, $i\neq j$) and the dilational strain ($\epsilon_{ij}=\epsilon_d>0$) below T_c [23,24] are given by

$$R_{1,2}^T=(3D_d^{v,c}+D_u^{v,c})\epsilon_d+2D_u^{v,c}\epsilon_s \tag{16}$$

for the singlet (T) valley and

$$R^{L}_{1,2} = (3D^{v,c}_{d} + D^{v,c}_{u})\epsilon_{d} - \tfrac{2}{3}D^{v,c}_{u}\epsilon_{s} \tag{17}$$

for the triplet (L) valley, where v and c denote the valence and conduction bands, respectively.

As already shown in equations (16) and (17), the shifts in the conduction and valence band edges in the rhombohedral phase towards their positions in the cubic phase are due to the acoustic deformation potential (D_d, D_u) and the rhombohedral strain (ϵ_d, ϵ_s) because

$$\Delta^{T} = R^{T}_{1} - R^{T}_{2} = [3(D^{c}_{d} - D^{v}_{d}) + D^{c}_{u} - D^{v}_{u}]\epsilon_{d} + 2(D^{c}_{u} - D^{v}_{u})\epsilon_{s} \tag{18}$$

for the singlet valley, and

$$\Delta^{L} = R^{L}_{1} - R^{L}_{2} = [3(D^{c}_{d} - D^{v}_{d}) + D^{c}_{u} - D^{v}_{u}]\epsilon_{d} - \tfrac{2}{3}(D^{c}_{u} - D^{v}_{u})\epsilon_{s} \tag{19}$$

for the triplet valley.

The values of the deformation potentials D_d and D_u are calculated theoretically from Ferreira [25] for PbTe ($D^{c}_{d} = -4.4$ eV, $D^{v}_{d} = -8.9$ eV, $D^{c}_{u} = 8.3$ eV and $D^{v}_{u} = 10.5$ eV) and from Rabii [26] for SnTe ($D^{c}_{d} = -7.56$ eV, $D^{v}_{d} = -4.88$ eV, $D^{c}_{u} = 7.35$ eV and $D^{v}_{u} = 7.98$ eV). The relative shifts in the valleys due to the optical distortion (the relative sublattice shift u) are given by [1]

$$\Delta^{vc} \simeq \Xi^{2}u^{2}/E^{*}_{g} \tag{20}$$

where E^{*}_{g} is the average band gap and Ξ is the optical phonon deformation potential.

If we summarize, the cubic–rhombohedral ferroelectric phase transition causes the following changes in the band-edge structure of IV–VI semiconductors [11,24]. The direct energy gap in the cubic phase is situated in the L points of the BZ. The surfaces of constant energy can be approximated by ellipsoids of revolution with their main axis oriented along the eight ⟨1 1 1⟩ directions. In the rhombohedral phase (below T_c) the symmetry of the four equivalent cubic L points (D_{3d} is reduced to three equivalent ones with C_s symmetry and one (C_{3v}) along the direction of the relative sublattice displacement. The corresponding BZ is shown in figure 2. The lowering in symmetry has three consequences for the band-edge structures.

(i) The band gap will be changed and the gaps close to the T and L points will be different.

(ii) The Fermi surfaces of each valley are distorted ellipsoids of revolution and their effective masses and anisotropies may be different for the L and T valleys.

(iii) The T–L splitting results in a carrier redistribution among the valleys below T_c.

3.3. The band structures of rhombohedral GeTe and its solid solutions

The transport coefficients in GeTe with carrier concentration $10^{20} \leqslant p \leqslant 10^{21}$ cm^{-3} are determined from carriers in the two valence bands (VB) with different densities of states: the band of light holes with density-of-states effective mass $1.2m_0$ and the band of heavy holes with density-of-states effective mass $4m_0$ to $5m_0$ (m_0 is the free-electron mass). The energetic distance between these two VB is about 0.27 to 0.30 eV. At room temperature the Fermi level enters the VB of the heavy holes at $p > 7 \times 10^{20}$ cm^{-3} [27]. Primarily the band of heavy holes was connected with the

Σ points of the BZ [28]. In the cubic phase it consists of 12 valleys with extrema situated on the axis [1 1 0]. For rhombohedral or orthorhombic distortions of a crystal the Σ valleys are split, too. The band-edge structure model of GeTe with parabolic extrema taking taking into account the splitting of L and Σ points in rhombohedral and orthorhombic phases is given by Korzheuv [1].

As the VB structures of GeTe–$AgBiTe_2$ SS have not been investigated until now, to explain the observed temperature dependences of its transport coefficients we supposed that, as in the analogous system GeTe–$AgSbTe_2$ [29], the rhombohedral SS retain not only the crystal structure [13] but also the band structure of GeTe.

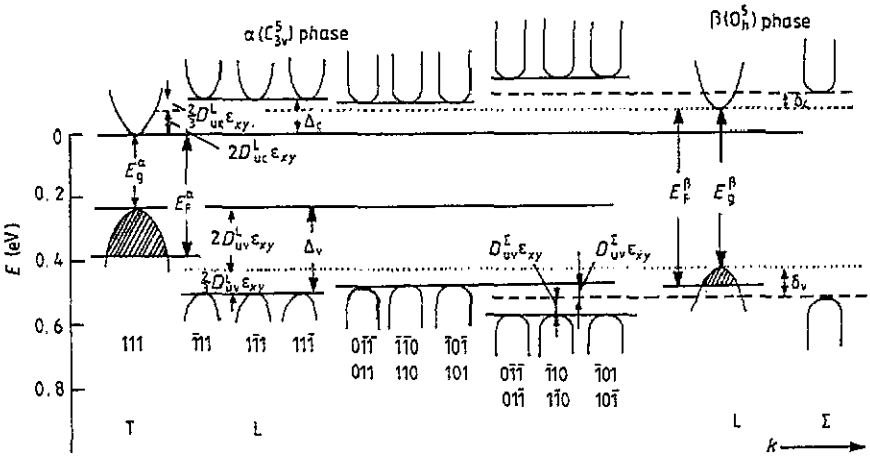

Figure 5. Germanium telluride band-edge model (300 K) with the splitting of four equivalent non-parabolic L extrema and 12 parabolic Σ extrema of the first Brillouin zone of the cubic lattice in ratio 1:3 (L) and 6:6 (Σ) due to the O_h^5–C_{3v}^5 phase transition in accordance with the results of figure 6.

Figure 5 shows the band-edge structure model of GeTe and investigated SS taking into account the splitting of the four equivalent non-parabolic L extrema and 12 parabolic Σ extrema of the first BZ of the cubic lattice in the ratios 1:3 (L) and 6:6 (Σ) due to the O_h^5–C_{3v}^5 phase transition in accordance with the experimental results on the lattice parameters [13] (see the following explanations).

The band gap of GeTe in the rhombohedral α phase, E_g^α (see figure 5), is taken as 0.23 eV at 300 K [28,29]. The energetic distance of the three L_v valleys (the subscript 'v' means the VB, 'c' CB and 'u' uniaxial) in the rhombohedral phase down to its position in the cubic phase is calculated from [1,30] (see also equations (16) and (17)):

$$\Delta^L = \tfrac{2}{3} D_{uv}^L \epsilon_{xy} \tag{21}$$

but that of the T_v valleys upwards to the conduction bands from

$$\Delta^T = 2 D_{uv}^L \epsilon_{xy} \tag{22}$$

where D_{uv}^L is the deformation potential constant for the L valleys of the VB, corresponding to uniaxial deformation of a crystal, taken equal to the value for

GeTe, $D^{L}_{uv} = 6.8$ eV [1]. The homogeneous rhombohedral shear strain ϵ_{xy} appears as an order parameter (second-order transition) and is given by [1]

$$\epsilon_{xy} = \tfrac{1}{2}\Delta\phi \simeq [(T_c - T)/T_c]^{\beta}. \tag{23}$$

Here β is the critical index of the order parameter and $\Delta\phi$ the deviation of the rhombohedral angle from $\pi/2$ (in radians). If the cubic structure of GeTe is retained to 300 K, the L_v valleys will be equivalent and their energetic distance to the CB top in the rhombohedral phase will be equal to (see figure 5).

$$E_g^{\alpha} + \Delta^{T} = 0.23 \text{ eV} + 0.1945 \text{ eV} = 0.4245 \text{ eV}. \tag{24}$$

The energetic position of the Σ_v valley top in the hypothetical cubic phase to the CB top in the rhombohedral phase (the zero level) will be given by (see figure 5)

$$\begin{aligned} E_g^{\alpha} + \Delta^{T} + \delta_v &= E_g^{\alpha} + 2D^{L}_{uv}\epsilon_{xy} + 2D^{\Sigma}_{uv}\epsilon_{xy} \\ &= 0.23 \text{ eV} + 0.1945 \text{ eV} + 0.944 \text{ eV} = 0.5189 \text{ eV}. \end{aligned} \tag{25}$$

The energetic distances from the zero level of the 12 parabolic Σ_v extrema of the first BZ of the rhombohedral lattice split in the ratio 6:6 down to its positions in the cubic phase are calculated from (see figure 5)

$$\Sigma_1 = E_g^{\alpha} + \Delta^{T} + \delta_v - D^{\Sigma}_{uv}\epsilon_{xy} \tag{26}$$

and

$$\Sigma_2 = E_g^{\alpha} + \Delta^{T} + \delta_v + D^{\Sigma}_{uv}\epsilon_{xy}. \tag{27}$$

For the ternary compound $AgBiTe_2$ with cubic (O_h^5) structure [31], the forbidden band-gap width is determined from the temperature dependence of the electrical conductivity (0.17 eV) and from the temperature dependence of the Hall coefficient (0.18 eV) [32]. The position of the Σ_v valley of $AgBiTe_2$ is unknown. It is taken equal to the position of the Σ_v valley of the analogous ternary compound $AgSbTe_2$, i.e. $\Sigma_v = 0.135$ eV [33] measured from the CB top (see figure 5). This seems to be possible because the crystal structure of both compounds is of the NaCl type with statistical distribution of the Ag and Bi (or Sb) ions on the cation sites [31] and the value of the position of the L_v valley (E_g) of $AgSbTe_2$ [33] is $L_v = 0.18$ eV (equal to E_g of $AgBiTe_2$ [32]). The position of the Fermi level is derived from the experimental value of the thermoelectric power, supposing that the two-band Kane model for narrow-gap semiconductors, especially for IV–VI compounds [15,34], is valid and taking into account the band non-parabolicity with modified Fermi–Dirac integrals [35]. The energetic positions of the T_v valley and the three L_v valleys in the rhombohedral phase ($0 \leqslant x \leqslant 0.23$) are determined from the experimental results of the SS inter-axial angle [13] using equations (22) and (23) and the deformation potential constant of GeTe, $\Xi^{L}_{u,v} = 6.8$ eV.

The results of these calculations at 300 K are presented in figure 6. The energetic positions of the Fermi level F (calculated from the experimental values of the thermoelectric power S) and of the T and L levels in the O_h^5 and C_{3v}^5 phase are measured from the CB of GeTe in the C_{3v}^5 phase (zero level), which is supposed constant with composition Z. The parameter $Z = 2x/(1+x)$ gives the number of impurity atoms (Ag and Bi) introduced into the cation sublattice. The number of Ge atoms is $1 - Z$. As can be seen, the positions of the L valleys and the Fermi level change with composition. They will change also with temperature. This determines the transport coefficient changes for SS.

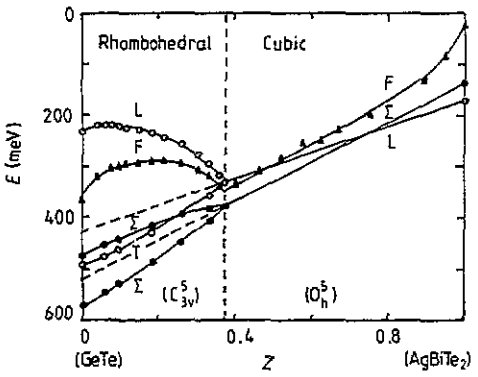

Figure 6. Interpolated band-edge structures of end compounds (GeTe and $AgBiTe_2$) for the GeTe–$AgBiTe_2$ system at 300 K. The splitting of L and Σ valleys as a result of the cubic–rhombohedral phase transition is taken into account. Energies are measured from the conduction band top in the rhombohedral phase. The calculated (from thermoelectric power S) positions of Fermi energies are also given with triangles. Full circles, Σ; open circles, L, T.

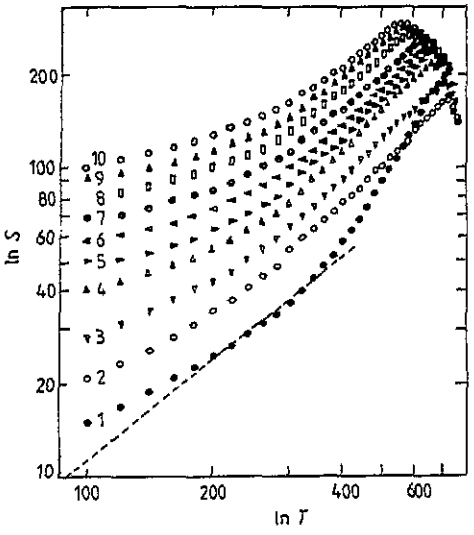

Figure 7. The temperature dependence of the thermoelectric power S of $(GeTe)_{1-x}(AgBiTe_2)_x$: (1) $x = 0$, (2) 0.02, (3) 0.04, (4) 0.06, (5) 0.08, (6) 0.10, (7) 0.12, (8) 0.15, (9) 0.18, (10) 0.20. Some of the curves (1, 6, 8 and 10) have been measured and discussed before [7]. T is measured in K, S in $\mu V\ K^{-1}$.

3.4. Thermoelectric power

In the case of GeTe [36] and GeTe-rich ss in the systems GeTe–MnTe [37] and GeTe–$AgSbTe_2$ [38], the temperature dependence of S was successfully explained by accepting that the thermoelectric power is the sum of diffusion and phonon-drag contributions,

$$S = S_e + S_l \tag{28}$$

and using the metallic expressions for S_e and S_l. The diffusion term S_e arises from the diffusion of the carriers (the holes in a single-valent T band, according to the band-edge structure of GeTe and GeTe-rich ss in the rhombohedral (C_{3v}^5) phase (see figures 5 and 6)). It can be considered to be proportional to the absolute temperature in the interval 77 to 300 K, and is given by [39]

$$S_e = AT = b_e C_e = (\pi^2 k_B/3e)(1/F^*) \tag{29}$$

where A and b_e are coefficients, C_e the electronic specific heat capacity, k_B the Boltzmann constant, $F^* = F/k_B T$ the reduced Fermi energy, e the electron charge and T the absolute temperature.

The phonon-drag term S_l has a complicated temperature dependence. In the temperature region $T \ll \theta_D/10$ (θ_D being the Debye temperature of the system) it is given by

$$S_l = BT^3 = b_l C_l \tag{30}$$

where b_l and B are coefficients, C_l is the lattice specific heat capacity, and T is the absolute temperature. For temperatures $T \gg \theta_D/10$, S_l must be proportional to the reciprocal temperature. At low temperatures the value of S_l is given in a first approximation by [40, 41]:

$$S_l = (C_l/3ep)/[1 + (\tau_{pe}/\tau_p)] \tag{31}$$

where p is the carrier density, C_l the lattice specific heat, τ_{pe} the phonon–carrier relaxation time, and τ_p the phonon relaxation time for all other scattering processes. This equation should more strictly be replaced by an integral over the complete phonon frequency spectrum. According to the theory [41] at high temperatures ($T > \theta_D$) the value of C_l should be constant and τ_{pe} is also independent of temperature since the dominant scattering mechanism, anharmonic phonon–phonon scattering, gives a relaxation time that is inversely proportional to temperature. It is possible to conclude that S_l should be inversely proportional to T in this temperature region.

Hence, for $T \ll \theta_D/10$ the measured thermoelectric power S should be given by

$$S = AT + BT^3 \tag{32}$$

and for $T \gg \theta_D/10$ it should be given by

$$S = AT + B'/T. \tag{33}$$

As in our measurements (77 to 900 K) the temperature region $T \ll \theta_D/10$ is not reached (θ_D of GeTe being $\simeq$ 200 K [42]), the temperature dependence of S must obey equation (35), and if the phonon-drag contribution S_l of the thermoelectric power is calculated the electronic part S_e must be separated. It must obey the expression [34]:

$$S_e = (k_B/e)[{}^1L_2^{r+3/2}(F^*, \beta)/{}^0L_2^{r+3/2}(F^*, \beta) - F^*] \tag{34}$$

where ${}^nL_k^m$ are modified Fermi–Dirac integrals of the type [35]

$${}^nL_k^m(F^*, \beta) = 3^{k/2}\int_0^\infty \left(-\frac{\partial f_0}{\partial X}\right) X^n(X + \beta X^2)^m[(1 + 2\beta X)^2 + 2]^{-k/2}\,dX \tag{35}$$

$\beta = k_BT/E_g$ is the non-parabolicity parameter, $X = E/k_BT$, and E_g is the direct energy gap. Those integrals give an account of the influence of non-parabolicity on the density-of-states energy dependence $\rho(E)$ and dispersion law $E(k)$ (k is the wavevector). The scattering index r is taken equal to -0.5 in accordance with the basic mechanisms of carrier scattering in IV–VI compounds [41] and investigated SS, i.e. scattering by acoustic phonons, point defects, impurity atoms and composition fluctuations. Equation (36) allows one to determine the values of F^* and F for the investigated SS.

4. Experimental results and discussion

The experimental $S(T)$ dependences of the investigated alloys (x = 0, 0.02, 0.04, 0.06, 0.08, 0.10, 0.12, 0.15, 0.18 and 0.20) are presented in figure 7. As can be seen, with increase of the amount of Ag and Bi atoms introduced in the cation sublattice (Z) the thermoelectric power increases in the whole temperature interval. Above

$\simeq$ 200 K (θ_D of GeTe being about 200 K [42]) a region of linear increase of S exists (see the broken tangent to the temperature dependence of S of GeTe) of width of about 100 to 200 K, which is shifted to higher temperatures with increasing $AgBiTe_2$ content in the alloys. The reason for this may be some decrease of the Debye temperature for solid solutions on substituting Ge atoms (atomic weight 72.5) in the cation sublattice by heavy Ag (atomic weight 107.868) and Bi (atomic weight 208.980) atoms. At temperatures above the upper limit of that region ($\simeq$ 400 K) a rapid increase of S is observed, which is connected with the transition into the high-temperature cubic (O_h^5) phase, and corresponding band changes.

If equation (35) for the temperature dependence of the thermoelectric power is obeyed in our case, then the plots of ST against T^2 should yield straight lines for $T \gg \theta_D/10$. The results obtained from such diagrams are shown in figure 8. Good straight lines are obtained in the temperature interval 77 K $< T <$ 250 K, illustrating equation (35), thus giving the values of A and B'. The derived values of A and B' of the investigated ss for different alloys are presented in figure 9 versus Z. The values of the phonon-drag coefficient B' (see equation (35)), different for every composition, increase linearly with increasing amount of introduced impurity atoms (Ag and Bi) replacing Ge in the cation sublattice and obey the law (see figure 9)

$$B' = (\tan\alpha)Z = CZ + D \tag{36}$$

where α is the angle between the straight lines and the axis of Z, $C \simeq 14$ mV/impurity atom and $D \simeq 0$, i.e. for GeTe $B' \simeq 0$, $S_1 \simeq 0$ in the temperature interval mentioned above.

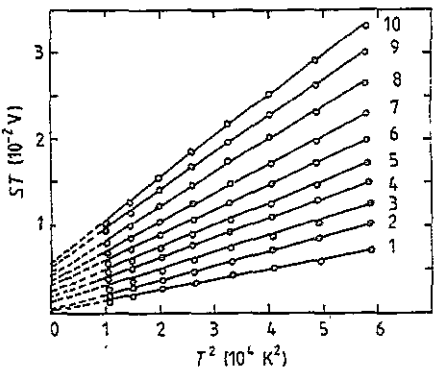

Figure 8. The plot of ST versus T^2 illustrating the validity of (33) in the temperature interval 100 to about 240 K. The compositions are marked as in figure 7.

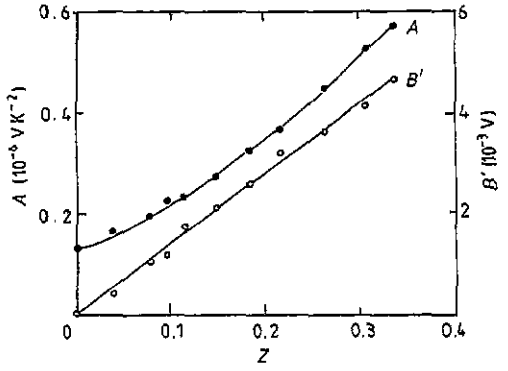

Figure 9. The variations of the coefficients A and B' in equation (33) versus composition Z.

The values of the diffusion term coefficient A (measured in μV K^{-2}) are also different for different alloys and increase with increasing Z. They obey the law

$$A = 1.892Z^2 + 0.721Z + 0.129. \tag{37}$$

If A is plotted versus the rhombohedral angle ϕ (measured at 300 K) it obeys a linear law with the intercept from the axis of A (figure 10). The reason for this must be the relation between the lattice strain, band structure, position of the Fermi level, the

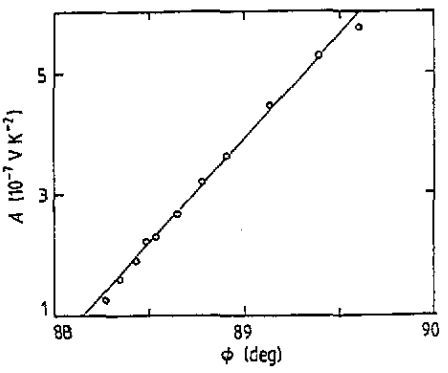

Figure 10. The variation of the phonon-drag coefficient A (equation (33) versus the rhombohedral angle ϕ.

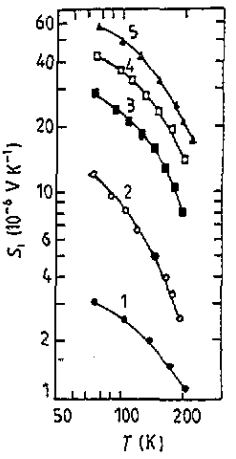

Figure 11. Temperature dependence of S_l derived from experimental $S(T)$ dependence in accordance with equation (33)): (1) $x = 0$, (2) 0.05, (3) 0.10, (4) 0.15, (5) 0.20.

number of carriers and their density-of-states effective mass, which are different for every composition, i.e. the result of interaction between two non-linear dependences ($A(Z)$ and $\phi(Z)$) is a linear one ($A(\phi)$).

The values of the diffusion term S_e may be derived by linear extrapolation of S from the temperature $\theta_D \leqslant T \leqslant 400$ K (for GeTe, $\theta_D \simeq 200$ K [42]) to low temperatures (broken part of curve 1, figure 7). The value of the phonon-drag component is derived as the difference between S and the value of S_e found in this manner ($S_l = S - S_e$) and is presented in figure 11 versus temperature for some compositions ($x = 0$, 0.05, 0.10, 0.15 and 0.20). For all investigated samples the sign of S_l is positive and the same as that of S_e. This shows the predominant role of inter-band scattering mechanisms at low temperatures in the $(GeTe)_{1-x}(AgBiTe_2)_x$ system as in the $Ge_{1-y}Te_y$ [36] and $(GeTe)_{1-x}(AgSbTe_2)_x$ systems [38].

The temperature dependence of S_l at $T > 77$ K is analogous to the results for $Ge_{1-y}Te_y$ [36] and for some GeTe–MnTe alloys [37], but we have not observed maxima of S_l at $T = \frac{1}{5}\theta_D$ to $\frac{1}{7}\theta_D$, probably because such temperatures ($\simeq 40$ to $\simeq 28$ K) are not reached in our measurements. A rapid increase of absolute value of S_l is observed, which is connected with the rapid decrease of carrier concentration upon increasing x [6]. Such an increase is observed in $Ge_{1-y}Te_y$ [36], GeTe–MnTe [37] and $(GeTe)_{1-x}(AgSbTe_2)_x$ [38] alloys.

The calculations show that the increase is a result of a simultaneous variation of p, τ_{pe} and τ_p (increase of τ_{pe}/τ_p in the second term of (31) for C_l constant). In ss it is possible also to observe an increase of C_l due to a decrease of the Debye temperature. The relatively small value of the scattering cross section of vacancies ($\simeq 10^{17}$ cm^2 [43]) is explained [36] by a large electron–phonon interaction in GeTe. The increase of S_l in $(GeTe)_{1-x}(AgBiTe_2)_x$ with increasing x is possibly a result of increasing electron–phonon interaction in the ss (decrease of T_c and τ_{pe}).

In the phase transition region ($T = T_c$) with $T_c \simeq 700$ K for GeTe [1] and $T_c \simeq 420$ K for ss $(GeTe)_{0.85}(AgBiTe_2)_{0.15}$ [31], no anomalous changes in the

thermoelectric power are observed. At $T_{max} > T_c$, S undergoes a maximum and after this it decreases. The relatively high values of S at the maximum are in agreement with the results of Bushmarina *et al* [6]. The value of S at the maximum increases with increasing content of $AgBiTe_2$ in the alloys and is shifted to lower temperatures. The first effect is connected with the decrease of carrier concentration, observed with increasing content of $AgBiTe_2$ [5], and the second one with decreasing temperature of the liquid and solids [3,4]. The existence of a region in which S decreases with increasing temperature at $T > T_{max}$ is evidence for the appearance of a carrier of opposite sign, i.e. the beginning of a region of intrinsic conductivity.

The derived values of the diffusion term $S_e(T)$ in the temperature interval 77 K $< T <$ 380 K are presented in figure 12. The curves for all compositions are not cut off, in the temperature interval mentioned above, i.e. the factors determining S change slowly with composition. With increasing temperature S_e deviates from a linear law and in the region from 240 to 280 K it is proportional to T^n with $1.2 < n < 1.7$ (see figure 12).

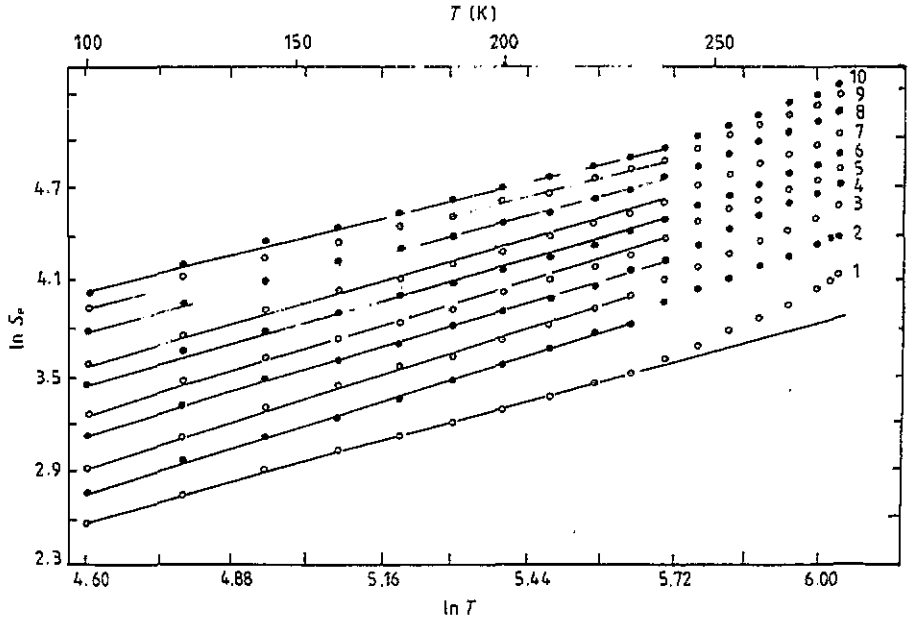

Figure 12. Temperature dependence of S_e. The compositions are marked as in figure 7. T is measured in K, S in μV K^{-1}.

To analyse the $S_e(T)$ dependences equation (30) must be used, but as it is very general it is difficult to apply for qualitative evaluations. The expression for S_e in some special cases will now be given.

In the case of a strongly degenerate semiconductor, when the current is determined by electrons with energies almost equal to the Fermi energy, the thermoelectric power is given by

$$S_e = (\pi^2/3)(k_B^2 T/e)[\partial \ln \sigma(E)/\partial E]_{E=F} \tag{38}$$

where $\sigma(E)$ is the energy dependence of the electrical conductivity. In the case of parabolic bands and a power law of the relaxation time, i.e. the case of a degenerate

semiconductor, from (38) one obtains

$$S_e = (\pi^2 k_B/3e)(r + 3/2)k_B T/F \tag{39}$$

which is equivalent to equation (29) at $r = -0.5$.

For non-degenerate semiconductors (39) transforms according to Pisarenco's formula,

$$S_e = (k_B/e)\left(r + \tfrac{5}{2}\right) + \ln[2(2\pi m_d^* k_B T)^{3/2}/\hbar^3 p]. \tag{40}$$

So for a degenerate semiconductor S_e is proportional to T, but for a non-degenerate one this dependence is weaker and changes according to a logarithmic law. It is clear now that to analyse the $S_e(T)$ dependence of SS the degree of degeneracy for every different alloy must be known. To reveal this, the Fermi energies are calculated by (34) from $S_e(T)$ data (see figure 11). It was supposed also that the transport coefficients are determined only by one type of carrier. The temperature dependences of E_g are taken equal to the dependences for GeTe and GeTe–$AgSbTe_2$ SS, i.e. $E_g = E_g(0) - 0.0004T$ in eV [43]. Then the minimum gap is $E_g = 0.11$ eV and the possible inaccuracy in the temperature coefficients, dE_g/dT, practically will not influence the experimental results (this is manifested by the non-parabolicity coefficient β).

Results for the Fermi energies at 300 K measured from the CB top are presented in figure 6. At $Z = 0$ (GeTe) the Fermi level lies deep in the VB and the alloys are degenerate semiconductors. With increasing Z the degeneracy decreases and the Fermi level reaches the VB top. At $Z > 0.5$ it enters the forbidden band.

It should be mentioned that the method of calculating the Fermi energy described above probably does not give the real picture because the transport coefficients for some compositions and in some temperature intervals are probably determined by two types of carriers. A qualitative consideration of the Fermi-level shift in this case will be given below.

The temperature dependences of the Fermi energy measured from the VB top calculated in this manner are presented in figure 13. For the investigated alloys with $0 \leqslant Z \leqslant 0.399$ at low temperatures the Fermi energy is constant. This region is nearly identical with the interval of the linear increase of the thermoelectric power. At temperatures lower than the temperature where the thermoelectric power deviates from the linear law, the Fermi energy appraoches the VB top, but with increasing Z the temperature limit of this region is shifted to lower temperature compared with GeTe (see figure 13). At finite temperatures decreasing with increasing $AgBiTe_2$ content, the Fermi energy enters the forbidden band (at room temperature at $Z > 0.5$, see figure 6).

Results for the reduced Fermi energies (figure 14) show that the compositions with $Z \leqslant 0.214$ ($x = 0.12$) are degenerate semiconductors ($F^* > 5$) at low temperatures. The degeneracy decreases with temperature increase. The compositions with $Z > 0.305$ ($x = 0.18$), on the whole temperature interval 77 to 360 K, are in the transition region between degenerate and non-degenerate semiconductors. This invalidated the calculations because of the impossibility of using the approximate formulae.

The GeTe-rich SS ($0 \leqslant Z \leqslant 0.399$) are characterized by a rhombohedral structure of the crystal lattice and a corresponding band-edge structure as was described in section 3.

In the temperature interval in which the Fermi energy lies deep in the VB (figure 13) the alloys are highly degenerate semiconductors ($F^* > 5$, broken line

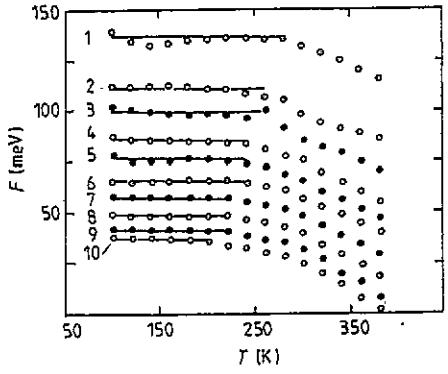

Figure 13. The calculated (from $S(T)$) temperature dependences of Fermi energy F measured from the VB top. The compositions are marked as in figure 7.

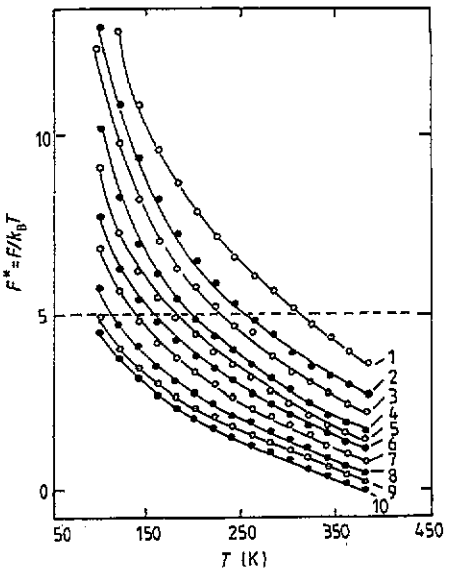

Figure 14. Calculated (from $S(T)$) temperature dependences of reduced Fermi energies. The compositions are marked as in figure 7.

in figure 14). If the splitting between the light- and heavy-hole bands is bigger than F, the Fermi level is situated in the light-hole VB, and this band is degenerate. In this case the temperature dependences of the thermoelectric power are determined by the light holes and are given by (39). According to this equation, if the energetic position of F is constant with temperature, S_e must be proportional to T. As can be seen from the experimental results (figures 13 and 14) this is observed in the temperature interval between 77 and 290 to 170 K. The upper limiting temperature of this interval is lower at bigger Z.

With increasing temperature and ternary compound content, a decrease of the rhombohedral lattice distortion occurs. The Fermi energy moves to the VB top and the splitting of the L and Σ bands (see figure 6) decreases. The bands of light and heavy holes approach each other. Carrier redistribution among the valleys occurs. The Fermi level moving near the VB top also results from the considerably higher heavy-hole density of states than that of the light holes. If the Fermi energy shift is taken into account, the observed deviation of the $S(T)$ dependence from the linear law at higher temperatures may be described by

$$S = (S_1\sigma_1 + S_2\sigma_2)/(\sigma_1 + \sigma_2) \tag{41}$$

where S_1 and S_2 and σ_1 and σ_2 are the thermoelectric power and electrical conductivity determined from the light and heavy holes, respectively. It is a pity that it is impossible to use this equation as the partial concentrations and mobilities of light and heavy holes are unknown.

It is interesting to note that the values of S_e at a constant value of T(T = 100, 200, 300, 400 and 500 K) as a function of the number of Ag and Bi atoms introduced in the cation sublattice lie on a family of straight lines (figure 15) with

increasing slope and intercepts (cuts) with increase of temperature. The reason for this is probably the slow change of the factor determining S at a constant temperature with composition (or at a constant composition with temperature).

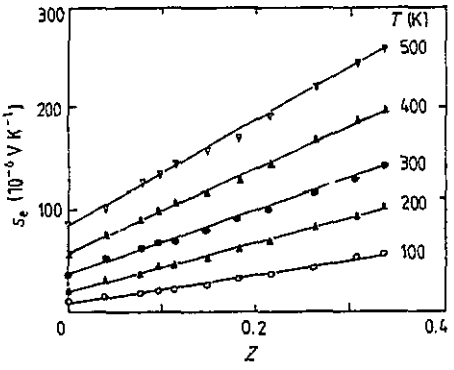

Figure 15. Electronic part of thermoelectric power at a constant temperature (T = 100, 200, 300, 400 and 500 K) versus the amount of the impurity Ag and Bi atoms, Z, in the cation sublattice.

5. Conclusions

The thermoelectric power for GeTe-rich $(GeTe)_{1-x}(AgBiTe_2)_x$ ss ($x \leqslant 0.20$) in the temperature interval 77 to $\simeq$ 400 K may be represented as the sum of a phonon-drag contribution dominant at lower temperatures ($T < \theta_D \simeq 200$ K) and a contribution from the degenerate hole gas dominant at higher temperatures ($T > \theta_D$). The deviations from a linear dependence at temperatures above the upper limit of that region are connected with the transition to the high-temperature cubic phase and corresponding band changes.

The existence of a region in which S decreases after it has reached a maximum is evidence for the beginning of the intrinsic conductivity region.

Results for the reduced Fermi energies ($F^* > 5$) show that the compositions with $Z \leqslant 0.214$ ($x \leqslant 0.12$) are degenerate semiconductors at low temperatures. The degeneracy decreases with a temperature increase. The compositions with $Z > 0.305$ ($x > 0.18$) on the whole temperature interval 77 to 360 K are in the transition region between degenerate and non-degenerate semiconductors ($F^* < 5$).

References

[1] Korzhuev M A 1986 *Tellurid Germania i Ego Fisicheskie Svoistva* (Moscow: Nauka)
[2] Abrikosov N Kh, Karpinskii O G, Shelimova L E and Korzhuev M A 1977 *Izv. Akad. Nauk SSSR, Ser. Neorg. Mater.* **13** 2160
[3] Plachkova S K, Odin I N, Sher A A and Novoselova A V 1980 *Izv. Akad. Nauk SSSR, Ser. Neorg. Mater.* **16** 1199
[4] Plachkova S K, Odin I N and Novoselova A V 1984 *Izv. Akad. Nauk SSSR, Ser. Neorg. Mater.* **20** 403
[5] Decheva St K, Dimitrova St K and Moralyiski P D 1975 *Bulg. J. Phys.* 2 350
[6] Bushmarina G S, Dedegkaev T T, Drabkin I A, Zhukova T B, Konstantinov P P, Lev E Ya and Sisoeva L M 1981 *Izv. Akad. Nauk SSSR, Ser. Neorg. Mater.* **17** 1392
[7] Plachkova S K 1985 *Phys. Status Solidi* a **92** 273
[8] Steenbeck M and Baranskii P I 1956 *Zh. Tekh. Fiz.* **26** 1373

[9] Gusach N and Kendel P 1958 *Proc. Phys. Soc.* **72** 898
[10] Kawamura H 1980 *Narrow Gap Semiconductors, Physics and Applications (Lecture Notes in Physics 133)* ed W Zavadski (Berlin: Springer) p 470
[11] Bauer G, Yantsch W and Bangert E 1983 *Festkörperprobleme (Advances in Solid State Physics XXIII)* (Braunschweig: Vieweg) p 27
[12] Plachkova S K, Georgieva O, Petrov K and Kovacheva D 1989 *Phys. Status Solidi* a **116** 213
[13] Plachkova S K, Shelimova L E and Karpinskii O G 1990 *Phys. Status Solidi* a **117** 155
[14] Plachkova S K and Georgieva O 1991 *Phys. Status Solidi* a **125** 503
[15] Kane E O 1957 *J. Phys. Chem. Solids* **1** 249
[16] Bauer G 1980 *Narrow Gap Semiconductors, Physics and Applications (Lecture Notes in Physics 133)* ed W Zavadski (Berlin: Springer) p 427
[17] Mitchell D L and Wallis R F 1966 *Phys. Rev.* **151** 581
[18] Dimmock Y O 1971 *The Physics of Semimetals and Narrow Gap Semiconductors* ed C L Carter and R T Bate (New York: Pergamon) p 319
[19] Bangert E 1981 *Physics of Narrow Gap Semiconductors (Lecture Notes in Physics 152)* ed E Gornik, H Heinrich and L Palmetshofer (Berlin: Springer) p 216
[20] He Yusheng and Grassie A D C 1985 *J. Phys. F: Met. Phys.* **15** 317, 337
[21] Bangert E 1983 according to [20]
[22] Herring C and Vogt E 1956 *Phys. Rev.* **101** 944
[23] Sugai S, Murase K, Tsuchihira T and Kawamura H 1979 *J. Phys. Soc. Japan* **47** 539
[24] Takaoka S and Murase K 1982 *J. Phys. Soc. Japan* **51** 1857
[25] Ferreira L G 1965 *Phys. Rev.* **137** A1601
[26] Rabii S 1969 *Phys. Rev.* **182** 821
[27] Kolomoetz N V, Lev E Ya and Sysoeva L M 1964 *Fiz. Tverd. Tela.* **6** 706; 1965 *Fiz. Tverd. Tela.* **7** 2223
[28] Lewis J E 1973 *Phys. Status Solidi* b **59** 367
[29] Baleva M I and Plachkova S K 1983 *J. Phys. C: Solid State Phys.* **16** 791
[30] Bir A S and Pikus G F 1972 *Simetria i Defonnazionnie Efecti v Poluprovodnikach* (Moscow: Nauka) p 516
[31] Geller S and Wernic Y H 1959 *Acta Crystallogr.* **12** 140
[32] Borisova L D and Dimitrova S K 1974 *C. R. Acad. Bulg. Sci.* **27** 1049
[33] Baleva M and Borisova L 1980 *Phys. Status Solidi* b **101** K57
[34] Ravich Yu I, Efimova B A and Smirnov I A 1968 *Metody Issledovanija Poluprovodnikov v Primenenii k Khalkogenidam Svintsa PbTe, PbSe, PbS* (Moscow: Nauka)
[35] Vassilev L V and Christakudis G Ch 1983 *Phys. Status Solidi* b **117** K53
[36] Korzhuev M A and Petrova L I 1982 *Fiz. Tekh. Poluprov.* **16** 1296
[37] Lewis J E, Rodot H and Haen P 1968 *Phys. Status Solidi* a **29** 743
[38] Plachkova S K 1983 *Phys. Status Solidi* a **80** K97
[39] Guenault A M 1967 *Phil. Mag.* **15** 17
[40] MacDonald D K C 1962 *Thermoelectricity—An Introduction to the Principles* (New York: Wiley)
[41] Blat F Y, Schroeder P A, Folies C L and Greig D 1976 *Thermoelectric Power of Metals* (New York: Plenum)
[42] Gogishvily O Sh, Ovsyanko I I and Yurchenk L I 1981 *Izv. Akad. Nauk SSSR, Ser. Neorg. Mater.* **17** 610
[43] Decheva-Plachkova S K 1983 *Phys. Status Solidi* b **119** K97